

Spin-orbit optical cross-phase-modulation

Etienne Brasselet*

Centre de Physique Moléculaire Optique et Hertzienne, Université Bordeaux I, CNRS, 351 Cours de la Libération, 33405 Talence Cedex, France

(Received 8 May 2010; revised manuscript received 27 October 2010; published 29 December 2010)

We show experimentally that optical phase singularities (PSs) can be written and erased, locally and in a controllable manner, into a light beam using the giant Kerr optical nonlinearities of liquid crystals. The method relies on the nonlinear optical spin-orbit coupling experienced by a collimated probe beam when a collinear focused pump beam imprints a radial birefringent pattern into a nematic film. In addition, experimental data are quantitatively described, accounting for the elastic anisotropy of the material and its nonlocal spatial response to the pump light field. Since we show that the optical intensity of a light beam (the “pump”) controls the phase of another beam (the “probe”) in a singular fashion (i.e., with the generation of a screw PS) via their interaction in a nonlinear medium that involves spin-orbit coupling, we dubbed such a nonlinear optical process as spin-orbit optical cross-phase-modulation.

DOI: [10.1103/PhysRevA.82.063836](https://doi.org/10.1103/PhysRevA.82.063836)

PACS number(s): 42.50.Tx, 42.60.Jf, 42.25.-p, 42.65.-k

I. INTRODUCTION

Optical nonlinearities are present in everyday life; an example being optical fiber communications [1]. Since quantum information based on the orbital angular momentum of light is expected to bring unprecedented opportunities to existing optical information protocols [2], the nonlinear control of the orbital degree of freedom of light fields should play an important role in future optical information technologies. Actually, optical nonlinearities are used to manipulate phase singularities (PSs) [3,4] or generate a PS itself [5,6] for over one decade, with an emphasis on screw PSs, which is explained from their connection with orbital angular momentum eigenstates of electromagnetic fields [7]. Such kinds of PSs correspond to a phase spatial distribution of the form $\exp(i\ell\phi)$, where ϕ is the azimuthal coordinate in the plane perpendicular to the propagation direction of the light and ℓ is called the topological charge. However, although it is known that the linear coupling between the spin (i.e., polarization) and the orbital (i.e., phase) degree of freedom of photons in uniaxial media (be they homogeneous [8] or spatially patterned in two [9] or three [10] dimensions) can efficiently generate PSs from Gaussian beams, we are unaware of any reports of its nonlinear control.

Here, we propose to combine the optical spin-orbit coupling process with a Kerr nonlinearity in order to control in a singular fashion (i.e., with the generation of a screw PS) the phase of a light beam (hereafter called the “probe”) with the optical intensity of another beam (the “pump”) via their interaction in a nonlinear medium. This introduces a novel nonlinear strategy toward on-demand optical generation or manipulation of screw PSs. Since the interaction of the pump and probe beams occurs via an optical spin-orbit coupling, we dubbed such a nonlinear optical process “spin-orbit optical cross-phase-modulation.” More precisely, we show experimentally that PSs can be written and erased, locally and in a controllable manner, into a (quasi) plane wave using the giant Kerr nonlinearities of liquid crystals [11]. The main idea consists

of benefiting from the local laser-induced axial patterning of the birefringence in nematic liquid crystal films using focused fundamental Gaussian beams—a possibility that was unveiled recently [12]. Our experiment relies on the local nonlinear spin-to-orbital angular momentum conversion experienced by a collimated probe beam, conditional on the presence of a collinear focused pump Gaussian beam that imprints a local (i.e., its amplitude decays away from the pumped area) axially symmetric birefringent pattern into a nematic film. This is illustrated in Fig. 1 for three different kinds of pump-driven optical-axis distributions in the transverse plane.

We note that the generation of a charge-two PS ($\ell = 2$) is expected from a geometric Pancharatnam-Berry phase, which arises from the continuous transverse changes of the optical axis with identical initial and final state all around the center of the modified area [13]. A simple quantitative understanding in terms of the Jones formalism in the case of a global (i.e. the optical axis orientation solely depends on the azimuthal angle) radial birefringent pattern can be found in Ref. [9]. This can also be understood from total angular momentum conservation since spin angular momentum flipping ($\pm\hbar \rightarrow \mp\hbar$) is associated to the appearance of a $\pm 2\hbar$ orbital angular momentum per photon that is related to a light beam endowed with a charge-two PS.

II. EXPERIMENT

The setup is depicted in Fig. 2. The pump light is generated from a cw TEM₀₀ laser source operating at wavelength $\lambda_1 = 532$ nm. Its propagation direction defines the z axis and its polarization state is set as circular using a quarter waveplate. The sample is a $L = 100$ - μm -thick nematic film (E7, from Merck) sandwiched between two 1-mm-thick glass substrates located at $z = z_{\text{in}}$ and $z = z_{\text{in}} + L$. The local averaged molecular axis orientation of the nematic is represented by a unit vector \mathbf{n} , called a director, and the refractive indices perpendicular and parallel to it are $n_{\perp} = 1.53$ and $n_{\parallel} = 1.77$, respectively. In the unperturbed state $\mathbf{n} = \mathbf{n}_0$, the nematic has a homogeneous alignment along the z axis.

An overfilled microscope objective with NA = 0.5 is used to focus the pump beam into a beam with waist and half

*e.brassellet@cpmoh.u-bordeaux1.fr

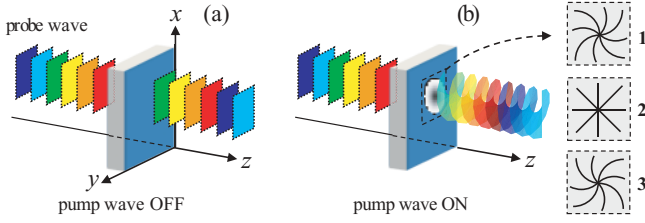


FIG. 1. (Color online) Illustration of spin-orbit optical cross-phase-modulation. Without the pump beam, the optical axis distribution of the sample lies along the z axis and the phase spatial distribution is therefore not modified (a). In contrast, a PS is locally generated where the axially symmetric laser-induced birefringent patterning takes place (b). Insets: three different kinds of pump-driven optical axis distributions in the (x,y) plane; inset 1 refers to left-handed circularly polarized pump beam, inset 2 refers to the case of radially polarized pump beam or to the incoherent collinear superposition of a left- and right-handed circularly polarized pump beam with same weight, and inset 3 refers to right-handed circularly polarized pump beam. The data presented in this work correspond either to case 1 or 3.

divergence at $\exp(-2)$ of its on-axis intensity $w'_0 \simeq 0.45 \mu\text{m}$ and $\theta'_0 \simeq 21.5^\circ$, respectively. We define the characteristic size of the pump beam intensity cross-section as the waist in the middle of the sample, $\langle w \rangle$. We have $\langle w \rangle = \langle z \rangle \tan \theta_0$ where $\langle z \rangle$ is the distance between the focal spot location and the central part of the film; see inset of Fig. 2, and $\theta_0 \simeq 14^\circ$ is the half divergence angle inside the sample accounting for the refraction. In this study, $100 < \langle z \rangle < 500 \mu\text{m}$, which gives $60 < \langle z \rangle / z_0 < 270$ with $z_0 = w_0 / \tan \theta_0$ ($w_0 = w'_0$) being the Rayleigh distance of the beam inside the sample.

The probe light is a cw TEM₀₀ collimated beam obtained from a He-Ne laser operating at $\lambda_2 = 632.8 \text{ nm}$ with a characteristic cross-section radius of the order of 1 cm and a \mathbf{e}_\pm circular polarization state; here $\mathbf{e}_\pm = (\mathbf{e}_x \pm i\mathbf{e}_y)/\sqrt{2}$ denotes the circular polarization basis in Cartesian coordinates. The intensity, polarization, and phase at the sample output are analyzed owing to a Mach-Zehnder interferometer scheme; see Fig. 2. In particular, the \mathbf{c}_\mp polarized component of the output

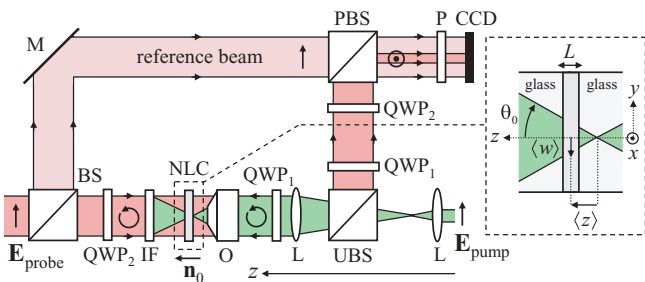


FIG. 2. (Color online) A circularly polarized pump beam (λ_1) is focused on a nematic film. The sample is probed by a collimated circularly polarized beam (λ_2) in a Mach-Zehnder configuration. QWP_{*i*}: quarter waveplate where the index *i* refers to λ_i ; L: lens; IF: interference filter for λ_1 ; O: microscope objective; NLC: nematic film; \mathbf{n}_0 : director at rest; BS: beam splitter; PBS/UBS: polarizing/unpolarizing beam splitter; P: polarizer; CCD: imaging device. Inset: half divergence, θ_0 ; characteristic waist inside the film, $\langle w \rangle$; distance from the focal spot location, $\langle z \rangle$.

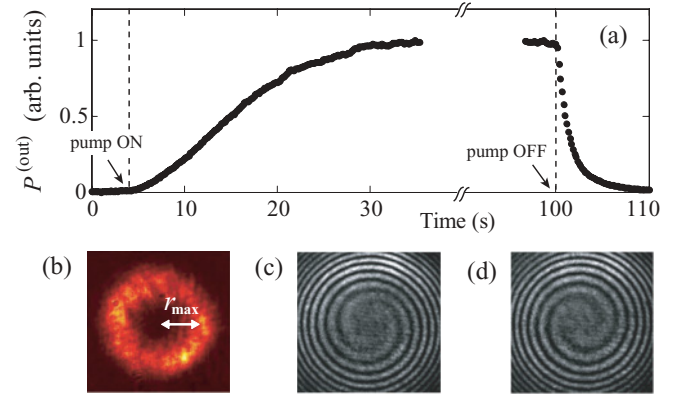


FIG. 3. (Color online) (a) Write and erase cycle for the total power carried by the light-induced optical vortex embedded in the output probe beam. (b) Typical doughnut intensity pattern of the nonlinearly generated vortex beam. (c), (d) Typical interference patterns between a reference beam with spherical wave front and the vortex beam for right- and left-circularly polarized probe beam.

probe beam is selected by means of a quarter waveplate and a polarizing beam splitter. As shown in Fig. 2, an additional quarter waveplate for λ_1 is inserted in order to compensate the phase delay introduced by the pump beam quarter waveplate.

In the unperturbed state $\mathbf{n} = \mathbf{n}_0$, both the polarization state and the spatial phase profile of the probe beam are unaltered when passing through the sample. When the pump is switched on, the director field is distorted and both radial and azimuthal reorientation modes appear. This leads to an axially symmetric local birefringent pattern $\mathbf{n} = \mathbf{n}_0 + \delta\mathbf{n}$ where $\delta\mathbf{n} = \delta n_r \mathbf{e}_r + \delta n_\phi \mathbf{e}_\phi + \delta n_z \mathbf{e}_z$ in a cylindrical coordinate system [12]. Experimentally, we observe a nonzero \mathbf{c}_\mp polarized probe component with total power $P_\mp^{(\text{out})}$; see Fig. 3(a). The associated intensity profile has a doughnut shape whatever the location $\langle z \rangle$ and pump beam power P_0 , see Fig. 3(b). Interferometric analysis of the phase spatial structure reveals a helical wavefront with topological charge two. As expected, its handedness only depends on the handedness of the probe beam polarization, as shown in Figs. 3(c) and 3(d) that correspond to right- and left-circularly polarized probe beam, respectively. Eventually, when the pump is switched off, the probe beam laser-induced modifications relax toward zero; see Fig. 3(a).

III. DATA ANALYSIS

Toward a quantitative analysis of the experimental data, we first retrieved the steady-state spatial structure of the vortex beam by measuring the radius of its circle of maximal intensity $r = r_{\text{max}}$ [see Fig. 3(b)], where r is the radial coordinate with the center pump beam as the origin. The experiment is performed for different values of $\langle z \rangle$ and, for the purpose of comparison with theory, we performed the measurements by imposing a constant maximal light-induced phase delay between the ordinary and extraordinary waves of the probe beam, $\Psi_{\text{max}} = \max[\Psi(r, \phi)]$ whatever $\langle z \rangle$, where $\Psi = \frac{2\pi}{\lambda_2} \int_{z_{\text{in}}}^{z_{\text{in}}+L} [n_e(\vartheta) - n_\perp] dz$ with $n_e(\vartheta) = n_\perp n_\parallel / (n_\parallel^2 \cos^2 \vartheta + n_\perp^2 \sin^2 \vartheta)^{1/2}$ and $\vartheta = \arcsin[(\delta n_r^2 + \delta n_\phi^2)^{1/2}]$. Results are

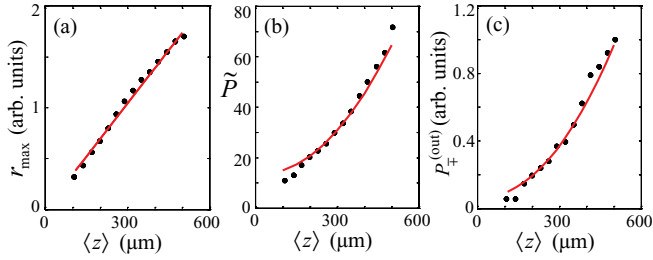


FIG. 4. (Color online) (a) Radius of the circle of maximal vortex beam intensity r_{\max} , (b) reduced power \tilde{P} , and (c) total power of the vortex beam $P_{\mp}^{(\text{out})}$ vs. $\langle z \rangle$ imposing $\Psi_{\max} \simeq 1.1$. Markers: experiment. Solid curves: theory. See text for the definitions of the different quantities.

shown in Fig. 4(a) for $\Psi_{\max} \simeq 1.1$. Obviously, the required pump power P_0 is all the more important than $\langle z \rangle$ is large since the nonlinearity is driven by the pump intensity, which scales as $\langle z \rangle^{-2}$ [see Fig. 4(b)]. The same trend is observed for the $\langle z \rangle$ dependence of the power $P_{\mp}^{(\text{out})}$ carried by the vortex; see Fig. 4(c).

In Fig. 4, we have introduced the reduced power $\tilde{P} = P_0/P_c$, where $P_c = K_3 n_{\perp} c / (n_{\parallel}^2 - n_{\perp}^2)$ is a characteristic power with c the speed of light and K_3 the bend elastic constant of the nematic. This choice arises from the resolution of the singular optical reorientation problem detailed in Ref. [14]. In the latter reference, however, the solution has been derived in the particular case $z_{\text{in}} = 0$ and solely for steady-state regimes under the assumption of the elastic isotropy. In the present work, we have generalized such a model in order to account for (i) any location $\langle z \rangle$ of the sample, (ii) elastic anisotropy, and (iii) dynamical features of the reorientation process, which implies the introduction of the dissipation function density in the Euler-Lagrange equations that now involve the rotational viscosity γ_1 [15]. Such a generalization, although cumbersome, is straightforward and, ensuing a new set of equations for the radial and azimuthal mode amplitudes $A_{r,\phi}$ and a characteristic spatial extent $w_{r,\phi}$ in the (x, y) plane, are therefore skipped here for the sake of conciseness. To summarize, the spatiotemporal characteristics of the generated optical vortex beam are retrieved from the knowledge of Ψ , which ultimately depends on $A_{r,\phi}$ and $w_{r,\phi}$ once the ansatz for the variational problem has been defined [14]. In particular, the intensity profile of the laser-induced vortex beam is obtained following $I_{\mp}^{(\text{out})} \propto \sin^2(\Psi/2)$ and its total power is $P_{\mp}^{(\text{out})} \propto \int_0^{\infty} \sin^2(\Psi/2) r dr$. In addition, the relaxation dynamics are found to have the following simple form in the limit of small reorientation amplitude, $A_{r,\phi}(t) = A_{r,\phi}(0) \exp[-\frac{K_3}{\gamma_1} (\frac{8\kappa_{1,2}}{w_{r,\phi}^2} + \frac{\pi^2}{L^2}) t]$, when the pump beam is switched off at time $t = 0$ and where $\kappa_1 = K_1/K_3$ and $\kappa_2 = K_2/K_3$ are the splay-to-bend and twist-to-bend elastic anisotropy ratios.

The experimental data in Fig. 4 can be fit using P_c as the single adjustable parameter in simulations that have been carried out using the material parameters $\kappa_1 = 0.69$ and $\kappa_2 = 0.36$. A satisfying agreement is found for $P_c = 11.5$ mW, as shown in Fig. 4. We note that this best-fit value corresponds to $K_3 = 20$ pN and falls in the typical range for nematics

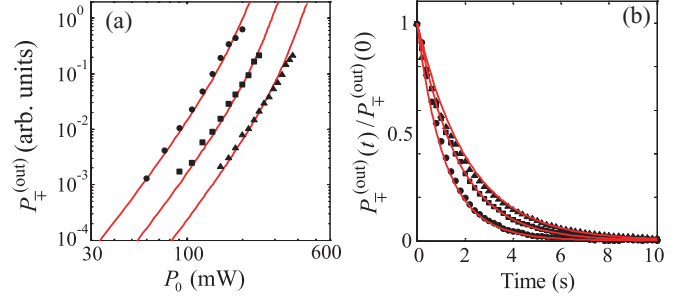


FIG. 5. (Color online) Vortex beam power vs. pump power (a) and relaxation dynamics from the steady state $\Psi_{\max} \simeq 1.1$ (b) for $\langle z \rangle = 170$ (circles), 260 (squares), and 350 μm (triangles). Markers: experiment. Solid curves: theory.

[15]. The dependence of $P_{\mp}^{(\text{out})}$ as a function of P_0 has also been investigated, as shown in Fig. 5(a) for $\langle z \rangle = 170$, 260 , and 350 μm . A good agreement between the predictions of the model and experimental data is found too. Finally, the relaxation from the steady state has also been studied, as shown in Fig. 5(b). Since Ψ , hence $P_{\mp}^{(\text{out})}$, explicitly depends on $A_{r,\phi}$, the viscoelastic ratio K_3/γ_1 is found to be the natural adjustable parameter to fit all the data (see above relaxation equations). The best-fit predictions give $K_3/\gamma_1 = 0.85 \times 10^{-10}$ $\text{m}^2 \text{s}^{-1}$, which agrees with measurements from other techniques [16] and are shown in Fig. 5(b).

Moreover, we observe optical vortices with higher-order radial modes at large power, see Fig. 6. These modes could be viewed as the analog of higher-order Laguerre-Gaussian modes $\text{LG}_{p,\ell}$, where p is the radial index and ℓ is the azimuthal index, when $p \neq 0$ [17]. The cases $p = (0, 1, 2)$ for $\ell = 2$ are shown in Figs. 6(a), 6(b), and 6(c), respectively. Our model also predicts such a behavior as demonstrated in Figs. 6(a'), 6(b'), and 6(c'), respectively. The agreement is, however, only qualitative due to the slightly broken symmetry observed for large p .

IV. DISCUSSION

Before concluding, a few remarks might be made. First, although liquid crystal materials are nonlocal nonlinear media, the proposed concept works too in the case of a local nonlinearity. Second, our results correspond to maximal intensities of the order of kW/cm^2 that are many orders of magnitude lower than the peak intensities used in harmonics

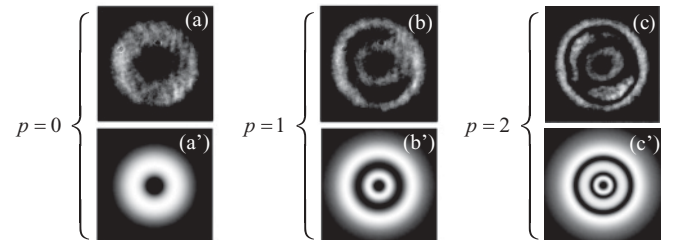


FIG. 6. Experimental (upper row) and calculated (bottom row) optical vortices with higher-order radial modes p for $\langle z \rangle = 260$ μm as the pump power increases (from left to right).

generation experiments based on electronic nonlinearities [3,4,6]. In fact, this is a direct consequence of the extremely high orientational nonlinearities of nematics. Nevertheless, such values could be further reduced by several orders of magnitude using more sensitive detection devices or larger optical nonlinearities, be they true (e.g., using dyes [18]) or effective (e.g., using photonic crystals [19]). Finally, we anticipate extension of the proposed strategy to other topological charges by using generalized cylindrical vector beams with the appropriate symmetry [20] or by using unconventional spatially engineered polarization states prepared with uniaxial crystals [21] for the pump beam. Finally, the present scheme can be also used to modify the topological charge of a vortex beam itself by using a probe beam that already carries PSs.

V. CONCLUSION

In summary, we have reported the experimental demonstration of rewritable, both in time and space, PSs based on the third-order optical nonlinearities of liquid crystals. All the observations have been quantitatively described with good agreement. Therefore, we have experimentally unveiled a nonlinear optical process, which we called spin-orbit optical cross-phase-modulation, that offers a strategy toward on-demand optical generation or manipulation of optical PSs. The reported phenomenon may be viewed as part of a more general class of nonlinear singular beam shaping that should also include self-induced aspects and which will be investigated in future work.

-
- [1] G. P. Agrawal, *Nonlinear Fiber Optics* (Academic, San Diego, 1989).
 - [2] G. Molina-Terriza, J. P. Torres, and L. Torner, *Nature Phys.* **3**, 305 (2007).
 - [3] K. Dholakia, N. B. Simpson, M. J. Padgett, and L. Allen, *Phys. Rev. A* **54**, R3742 (1996).
 - [4] A. Beržanskis, A. Matijošius, A. Piskarskas, V. Smilgevičius, and A. Stabinis, *Opt. Commun.* **140**, 273 (1997).
 - [5] S. Baluschev, A. Dreischuh, I. Velchev, S. Dinev, and O. Marazov, *Phys. Rev. E* **52**, 5517 (1995).
 - [6] M. Beresna, P. G. Kazansky, M. B. Y. Svirko, and R. Danielius, *Appl. Phys. Lett.* **95**, 121502 (2009).
 - [7] L. Allen, M. W. Beijersbergen, R. J. C. Spreeuw, and J. P. Woerdman, *Phys. Rev. A* **45**, 8185 (1992).
 - [8] A. Volyar and T. Fadeyeva, *Opt. Spectrosc.* **94**, 235 (2003).
 - [9] L. Marrucci, C. Manzo, and D. Paparo, *Phys. Rev. Lett.* **96**, 163905 (2006).
 - [10] E. Brasselet, N. Murazawa, H. Misawa, and S. Juodkazis, *Phys. Rev. Lett.* **103**, 103903 (2009).
 - [11] N. V. Tabiryan, A. V. Sukhov, and B. Y. Zel'dovich, *Mol. Cryst. Liq. Cryst.* **136**, 1 (1986).
 - [12] E. Brasselet, *Opt. Lett.* **34**, 3229 (2009).
 - [13] G. Biener, A. Niv, V. Kleiner, and E. Hasman, *Opt. Lett.* **27**, 1875 (2002).
 - [14] E. Brasselet, *J. Opt.* **12**, 124005 (2010).
 - [15] P. G. de Gennes, *The Physics of Liquid Crystals* (Oxford University Press, Oxford, 1974).
 - [16] G. Cipparone, D. Duca, C. Versace, C. Umeton, and N. V. Tabiryan, *Mol. Cryst. Liq. Cryst.* **266**, 263 (1995).
 - [17] J. Arlt, K. Dholakia, L. Allen, and M. J. Padgett, *J. Mod. Opt.* **45**, 1231 (1998).
 - [18] I. C. Khoo, *Phys. Rep.* **471**, 221 (2009).
 - [19] A. E. Miroshnichenko, E. Brasselet, and Y. S. Kivshar, *Phys. Rev. A* **78**, 053823 (2008).
 - [20] Q. Zhan, *Adv. Opt. Photon.* **1**, 1 (2009).
 - [21] T. A. Fadeyeva, V. G. Shvedov, Y. V. Izdebskaya, A. V. Volyar, E. Brasselet, D. N. Neshev, A. S. Desyatnikov, W. Krolikowski, and Y. S. Kivshar, *Opt. Express* **18**, 10848 (2010).